COBEM 2021 26th International Congress of Mechanical Engineering
ABCM Associação Brasileira de Engenharia e Ciências Mecânicas
November 22-26, 2021, Virtual Congress, Brazil

COBEM2021-1582
ESTIMATION OF THE BRAIN TEMPERATURE IN DEEP BRAIN STIMULATION APPLICATION WITH THE PARTICLE FILTER METHOD

Caroline R. Pereira[1]
Luiz A. S. Abreu[2]
Diego C. Knupp[3]
Lucas C. S. Jardim[4]
Polytechnic Institute, Rio de Jeneiro State University (IPRJ/UERJ), Nova Friburgo, RJ, Brazil
[1]rpereiracaroline@iprj.uerj.br; [2]luiz.abreu@iprj.uerj.br; [3]diegoknupp@iprj.uerj.br;[4]ljardim@iprj.uerj.br

Abstract. *Deep Brain Stimulation (DBS) is a medical therapy that involves sending electrical pulses to specific brain areas using electrodes implanted inside the brain. Although DBS is widely used around the world, some brain injuries could be related to internal burns and non-expected hot spots around the electrodes. This work deals with the sequential estimation of the internal temperature of the brain containing a DBS lead by solving a state estimation problem with the Particle Filter methods. The classical bidimensional bioheat equation was considered to model this problem. The associated direct problem was solved with a finite element approach implemented through the NDSolve function, intrinsic to the Mathematica software, and this solution was verified with the Generalized Integral Transform Technique (GITT). The state estimation problem was solved with two particle filters: the Sampling Importance Resampling (SIR) algorithm and the Liu & West's algorithm. Experimental temperatures were obtained supposedly with a sensor located inside the brain electrode. Uncertainties in the evolution and observation models were assumed as additive, Gaussian, uncorrelated and with zero means. The results were obtained considering simulated temperature measurements, with different noise levels and accurate estimations were obtained. The results showed a promising approach to reducing the risks of lesions related to the Deep Brain Stimulation technique.*

Keywords: *deep brain stimulation, bioheat transfer, inverse problem, particle filter methods*

1. INTRODUCTION

Deep Brain Stimulation (DBS) is a well-established medical therapy that involves sending electrical pulses to specific brain areas using electrodes implanted inside the brain (Elwassif *et al.*, 2006, 2012; Cubo and Medvedev, 2018; Aum and Tierney, 2018; Jardim *et al.*, 2020). The procedure is performed to stimulate the functioning of the organ and improve the performance and quality of life of people who have neurological diseases such as Parkinson's disease (Starr *et al.*, 1998; Xiao *et al.*, 2020), epilepsy (Salanova, 2018), Alzheimer's disease(Lam *et al.*, 2021), and others (Aum and Tierney, 2018; Krauss *et al.*, 2004). However, despite DBS being widely used around the world and having a well-tolerated surgical procedure, little is known about its physiological effects on the brain. Some of the most common injuries are related to possible internal burns from thermal coupling with other equipment, such as magnetic resonance imaging (MRI) (Elwassif *et al.*, 2006, 2012; Jardim *et al.*, 2020).

Thus, the temperature changes induced by DBS are of broad interest and need to be controlled to minimize the risk of injury. These variations were analyzed by solving direct problems considering approximate mathematical models of the brain (Chang, 2003; Elwassif *et al.*, 2006, 2012) or even more realistic models obtained from MRI (Khadka *et al.*, 2020). There are also studies to monitor temperature rise by solving direct problems in other parts of the human body and even in the brain that use mathematical models similar to the DBS model (Fiocchi *et al.*, 2020).

Furthermore, inverse problem techniques that take into account experimental measurements can be used to estimate some physical properties present in the mathematical DBS model, as was done by Jardim *et al.* (2020).The use of inverse problems for parameter estimation and obtaining the temperature field is quite relevant, since it allows the insertion of uncertainties associated with the mathematical model and properties in the problem, in addition to taking into account experimental measurements. In this context, inverse problem solving using Bayesian filters has been used in bioheat transfer problems. Several papers can be found employing state estimation problems to obtain the temperature field in hyperthermic cancer treatments in different parts of the human body (Lamien *et al.*, 2017a,b; Nunes *et al.*, 2020; Pacheco *et al.*, 2020), cerebral ischemia (Nunes *et al.*, 2019), and others (Pacheco *et al.*, 2018).

In this context, to the authors' knowledge, there is no publication where particle filtering methods have been applied to

problems involving DBS. Thus, this study aims to show the possibility of sequentially estimating the internal temperature field of the brain containing a DBS electrode by solving a state estimation problem using a particle filter algorithm. The physical problem and the mathematical formulation discussed in this article are presented in the next section, which is followed by the direct solution of the problem with `NDSolve` and GITT, by the algorithm for solving the state estimation problem, by the results obtained with the direct and inverse problems and by the conclusions of this work.

2. PHYSICAL PROBLEM AND MATHEMATICAL FORMULATION

The physical problem considered in this paper involves the bioheat transfer in the brain with an implanted DBS electrical stimulator. Assuming that the problem has symmetry, the solution reduces to solving the case of an axisymmetric plane defined by the length of the conductor and the radius of a cylindrical coordinate system, as illustrated in Fig. 1(a). This plane has boundaries ranging from $r = R_1$ to $r = R_2$ and from $z = 0$ to $z = H$, where R_1 is the radius of the electrode, R_2 and H are, respectively, a distance and a height long enough not to influence the solution of the computational simulation. In addition, it is considered that there is a sensor located in the center of the electrode, used to obtain experimental temperature measurements. The temperature rise will be described with the model proposed by Pennes (Pennes, 1948; Chang, 2003; Elwassif *et al.*, 2006, 2012; Jardim *et al.*, 2020; Khadka *et al.*, 2020):

$$\rho c_p \frac{\partial T}{\partial t} = \frac{1}{r}\frac{\partial}{\partial r}\left(kr\frac{\partial T}{\partial r}\right) + \frac{\partial}{\partial z}\left(k\frac{\partial T}{\partial z}\right) - \rho_b \omega_b c_b (T - T_b) + Q_m + Q_{ext}(r,z), \tag{1}$$

$$\left.\frac{\partial T}{\partial r}\right|_{r=R_1} = 0; \quad T(r,z,t) = T_a, \ \text{ at } \ r = R_2, \ z = 0, \ z = H \text{ and } t = 0, \tag{2}$$

where, for brain tissue, ρ is the specific mass, c_p is the specific heat, k is the thermal conductivity, and Q_m is the metabolic heat generation and, for the blood, ρ_b is the specific mass, ω_b is the perfusion, c_b is the specific heat, and T_b is the temperature. T_a is the initial temperature of the brain when there is no electrical heating. The term $Q_{ext}(r,z)$ represents the rate of heat supplied by an external source. In this case, the heating imposed by radiofrequency waves through electrodes implanted in the brain (Chang, 2003; Elwassif *et al.*, 2006, 2012; Lamien *et al.*, 2017b; Jardim *et al.*, 2020; Khadka *et al.*, 2020). Thus,

$$Q_{ext}(r,z) = \sigma |\nabla V|^2, \tag{3}$$

where σ is the electric conductivity, ∇V the electric field, and $V(r,z)$ the electric potential, obtained by solving the following Laplace equation (Chang, 2003; Elwassif *et al.*, 2006, 2012; Lamien *et al.*, 2017b; Cubo and Medvedev, 2018; Jardim *et al.*, 2020; Khadka *et al.*, 2020):

$$\frac{1}{r}\frac{\partial}{\partial r}\left(\sigma r\frac{\partial V}{\partial r}\right) + \frac{\partial}{\partial z}\left(\sigma\frac{\partial V}{\partial z}\right) = 0, \tag{4}$$

$$\frac{\partial V}{\partial \boldsymbol{n}} = 0, \ \text{ at } \ r = R_2, \ z = 0 \ \text{ and } z = H; \quad V(r,z) = f(z), \ \text{ at } \ r = R_1. \tag{5}$$

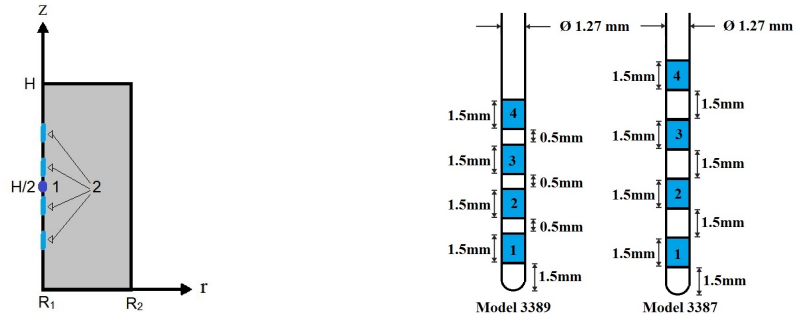

(a) The axisymmetric domain where 1 and 2 are the positions of the sensor and electrodes, respectively.

(b) Geometric configuration of the electrodes. Source: Adapted from Medtronic and INC (2002).

Figure 1. Schematic representation of the domain and electrodes.

The function $f(z)$ will be defined according to the electrode model used. For the result analysis, two Medtronic® DBS leads are studied: Model 3387 and Model 3389. These models are 1.27 mm diameter cylindrical, and in each one there are four electrodes with 1.5 mm length. The difference between them is the spacing of the electrodes, with distances of 0.5 mm for Model 3389 and 1.5 mm for Model 3387, as shown in Fig. 1(b) (Medtronic and INC, 2002).

3. SOLUTION OF THE DBS HEATING PROBLEM

The problem given by Eqs. (1) - (5) was solved with the Finite Element Method (FEM) implemented using a subroutine of the `NDSolve` function, intrinsic to the symbolic computing software Wolfram Mathematica®, which is used here with an automatic absolute and relative error control (Wolfram, 2021). The direct solution problem obtained with `NDSolve` was verified with the Generalized Integral Transformation Technique (GITT), described below.

In the direct problem a filter, given by Eq. (6), is applied to hasten the convergence of the solution. Thus, the final result will be the sum of the initial temperature T_a and the solution of the filtered problem given by Eqs. (7) and (8).

$$T(r,z,t) = T_a + T^*(r,z,t), \tag{6}$$

$$\frac{1}{\alpha}\frac{\partial T^*(r,z,t)}{\partial t} = \frac{1}{r}\frac{\partial T^*(r,z,t)}{\partial r} + \frac{\partial^2 T^*(r,z,t)}{\partial r^2} + \frac{\partial^2 T^*(r,z,t)}{\partial z^2} - \frac{\rho_b \omega_b c_b}{k}[T^*(r,z,t) + T_a - T_b] + \frac{Q_m}{k} + \frac{Q_{ext}(r,z)}{k}, \tag{7}$$

$$\left.\frac{\partial T^*(r,z,t)}{\partial r}\right|_{r=R_1} = 0; \quad T^*(r,z,t) = 0, \text{ at } r = R_2,\ z = 0,\ z = H \text{ and } t = 0, \tag{8}$$

where $\alpha = k/(\rho c_p)$. Thus, the filtered problem to be solved will have homogeneous boundary conditions, and GITT will be applied. Following the classical integral transform formalism for the solution of Eqs. (7) and (8), the following integral transform pair is proposed (Cotta *et al.*, 2018):

$$\text{Transform:} \quad \overline{T}_i(t) = \frac{1}{\alpha}\int_{R_1}^{R_2}\int_0^H \tilde{\psi}_i(r,z) T^*(r,z,t) dr dz, \tag{9}$$

$$\text{Inversion:} \quad T^*(r,z,t) = \sum_{i=1}^{\infty} \overline{T}_i(t)\tilde{\psi}_i(r,z), \tag{10}$$

with

$$\tilde{\psi}_i(r,z) = \frac{\psi_i(r,z)}{\sqrt{N_i}}; \quad N_i = \frac{1}{\alpha}\int_0^H \int_{R_1}^{R_2} \psi_i^2(r,z) dr dz, \tag{11}$$

where $\psi(r,z)$ are the eigenfunctions that come from the Sturm-Liouville eigenvalue problem obtained by considering the homogeneous version of Eqs. (7) and (8), given by Eqs. (12) and (13) (Cotta *et al.*, 2018).

$$\frac{1}{r}\frac{\partial \psi(r,z)}{\partial r} + \frac{\partial^2 \psi(r,z))}{\partial r^2} + \frac{\partial^2 \psi(r,z)}{\partial z^2} + \frac{\eta^2}{\alpha}\psi(r,z) = 0\ , \tag{12}$$

$$\left.\frac{\partial \psi(r,z)}{\partial r}\right|_{r=R_1} = 0; \quad \psi(r,z) = 0, \text{ at } r = R_2,\ z = 0 \text{ and } z = H. \tag{13}$$

Operating Eq. (7) with $\int_{R_1}^{R_2}\int_0^H \tilde{\psi}_i(r,z)(.) dr dz$, making use of orthogonality property of the eigenfunctions, and employing the boundary condictions leads to the following transformated problem (Cotta *et al.*, 2018):

$$\frac{d\overline{T}_i(t)}{dt} + \eta_i^2 \overline{T}_i(t) = \overline{g}_i(t, \overline{T}_i(t)), \quad i = 1, 2, ... \tag{14}$$

$$\overline{T}_i(0) = 0, \quad i = 1, 2, ... \tag{15}$$

$$\overline{g}_i(t, \overline{T}_i(t)) = \int_{R_1}^{R_2}\int_0^H \tilde{\psi}_i(r,z)\left\{ - \frac{\rho_b \omega_b c_b}{k}[T^*(r,z,t) + T_a - T_b] + \frac{Q_m}{k} + \frac{Q_{ext}(r,z)}{k}\right\} dr dz \tag{16}$$

$\psi(r,z)$ will be obtained by doing $\psi(r,z) = \varphi(r)\chi(z)$, with the following associated eigenvalue problems:

$$\frac{d^2\varphi(r)}{dr^2} + \frac{1}{r}\frac{d\varphi(r)}{dr} + \frac{\lambda^2}{\alpha}\varphi(r) = 0, \quad R1 < r < R2 \tag{17}$$

$$\frac{d\varphi(r)}{dr} = 0, \text{ at } r = R_1; \quad \varphi(r) = 0, \text{ at } r = R_2 \tag{18}$$

and

$$\frac{d^2\chi(z)}{dz^2} + \frac{\beta^2}{\alpha}\chi(z) = 0, \quad 0 < z < H \tag{19}$$

$$\chi(z) = 0, \text{ at } z = 0 \text{ and } z = H. \tag{20}$$

Moreover, the solution of these problems given by the eigenfunctions $\varphi_j(r)$ and $\psi_l(z)$, where $\psi_i(r,z) = \varphi_j(r)\chi_l(z)$, and by the eigenvalues λ_j and β_l, where $\eta_i^2 = \lambda_j^2 + \beta_l^2$, will be (Mikhailov and Ozisik, 1984):

$$\begin{aligned} &\varphi_j(r) = J_0\left(\tfrac{\lambda_j}{\sqrt{\alpha}}r\right)Y_0\left(\tfrac{\lambda_j}{\sqrt{\alpha}}R_2\right) - J_0\left(\tfrac{\lambda_j}{\sqrt{\alpha}}R_2\right)Y_0\left(\tfrac{\lambda_j}{\sqrt{\alpha}}r\right); \\ &J_0'\left(\tfrac{\lambda_j}{\sqrt{\alpha}}R_1\right)Y_0\left(\tfrac{\lambda_j}{\sqrt{\alpha}}R_2\right) - J_0\left(\tfrac{\lambda_j}{\sqrt{\alpha}}R_2\right)Y_0'\left(\tfrac{\lambda_j}{\sqrt{\alpha}}R_1\right) = 0, \end{aligned} \tag{21}$$

and

$$\chi_l(z) = sin\left(\frac{\beta_l}{\sqrt{\alpha}}z\right); \quad sin\left(\frac{\beta_l}{\sqrt{\alpha}}H\right) = 0. \tag{22}$$

In addition, the eigenvalues will be reordered in order to ensure that the values of $\eta_i = \sqrt{\lambda_j^2 + \beta_l^2}$ that contribute most significantly to the solution are added first. This way, we will have a simple summation where the index i will give the reordered λ_j and β_l values (Cotta *et al.*, 2013).

The solution to $Q_{ext}(r,z)$, Eq. (3), will come from the solution of Laplace's equation, Eq. (4) and (5), using separation of variables with $V(r,z) = R(r)Z(z)$ as shown below (Mikhailov and Ozisik, 1984).

$$\frac{1}{Z(z)}\frac{d^2Z(z)}{dz^2} = -\left[\frac{1}{rR(r)}\frac{dR(r)}{dr} + \frac{1}{R(r)}\frac{d^2R(r)}{dr^2}\right] = -\mu^2 \tag{23}$$

$$R(r)Z(z) = f(z), \text{ at } r = R_1; \quad \frac{dR(r)}{dr} = 0, \text{ at } r = R_2; \quad \frac{dZ(z)}{dz} = 0, \text{ at } z = 0 \text{ and } z = H, \tag{24}$$

Solving Eq. (23) with the boundary conditions, Eq. (24), the solution is givin by

$$V(r,z) = \frac{1}{H}\int_0^H f(z)dz + \sum_{n=1}^{\infty} C_n\left[I_0(\mu_n r) - \frac{I_0'(\mu_n R_2)}{K_0'(\mu_n R_2)}K_0(\mu_n r)\right]cos(\mu_n z) \tag{25}$$

with

$$sin(\mu_n H) = 0; \qquad C_n = \frac{\int_0^H f(z)cos(\mu_n z)dz}{\left[I_0(\mu_n R_1) - \frac{I_0'(\mu_n R_2)}{K_0'(\mu_n R_2)}K_0(\mu_n R_1)\right]\int_0^H cos^2(\mu_n z)dz}, \quad n = 1, 2, ... \tag{26}$$

Finally, the solution for the electric potential, Eq. (25), is derived and substituted into Eq. (3). Next, the transformed potentials were obtained numerically by employing the built-in routine `NDSolve`. Thus, the solution for $T^*(r,z,t)$ was reached utilizing the inversion formula, Eq. (10). Thus, the final solution for the biological tissue temperature is achieved by applying Eq. (6). All summations are truncated to order N large enough to obtain the required accuracy.

4. STATE ESTIMATION PROBLEM AND PARTICLE FILTER METHOD

State estimation problems have been developed so that available measured data can be used in conjunction with prior knowledge about physical phenomena, geometric parameters, and information regarding measurement devices in order to sequentially produce estimates of desired dynamic variables. These problems can be written in the form of evolution and observation models, which are modeled as stochastic processes. The evolution model, Eq. (27), describes the system evolution of the state variable over time, while the observation model, Eq. (28), is related to the available experimental measurements (Orlande *et al.*, 2011, 2008; Lamien *et al.*, 2017b; Nunes *et al.*, 2019).

$$\mathbf{x}_k = \boldsymbol{f}_k(\mathbf{x}_{k-1}, \boldsymbol{\theta}, \boldsymbol{v}_k), \quad k = 1, ..., M \tag{27}$$

$$\mathbf{z}_k = \boldsymbol{g}_k(\mathbf{x}_k, \boldsymbol{\theta}, \boldsymbol{n}_k), \quad k = 1, ..., M, \tag{28}$$

where $\mathbf{x}_k$ is the state vector which contains all the state variables that describe the system at a given time instant t_k, $\mathbf{z}_k$ is the prediction of the measurements ($\mathbf{z}_k^{meas}$), $\boldsymbol{\theta}$ is the parameter vector of the problem, and $\boldsymbol{v}_k$ and $\boldsymbol{n}_k$ represent the noises in the state evolution model and in the observation model, respectively. The objective of the state estimation problem is to obtain information about the state vector $\mathbf{x}_k$ based on the evolution and observation models defined by Eqs. (27) and (28), considering a probability density $\pi(\mathbf{x}_0, \boldsymbol{\theta}|\mathbf{z}_0) = \pi(\mathbf{x}_0, \boldsymbol{\theta})$ known at the initial time t_0 (Orlande *et al.*, 2011, 2008; Lamien *et al.*, 2017b; Nunes *et al.*, 2019).

These estimates can be made with Bayesian filters, which are probabilistic methods that use a recursive algorithm to estimate and update the states (Orlande *et al.*, 2011, 2008; Lamien *et al.*, 2017b; Nunes *et al.*, 2019). There are several types of Bayesian filters, for example, the Kalman filter and particle filters. The Kalman filter is used in Gaussian models and linear problems or where it is possible to linearize it (Orlande *et al.*, 2011, 2008). The particle filters is a powerful and robust technique that can be applied both in linear and nonlinear problems and non-Gaussian models (Nunes *et al.*, 2019; Lamien *et al.*, 2017b). For this problem, was chosen the particle filter. The particle filter method is a Monte Carlo technique for the solution of state estimation problems, in which the posterior probability density function is represented by a set of random samples (particles) with associated weights. In this case, the particles filter chosen were the Sampling Importance Resampling (SIR) algorithm, described in Tab. 1, and the Liu & West's algorithm, described in Tab. 2.

Table 1. Sampling Importance Resampling (SIR) algorithm (Orlande *et al.*, 2011, 2008; Nunes *et al.*, 2019).

Step 1
For $i = 1, ...N$, where N is the number of particles, draw new particles $\mathbf{x}_k^i$ from the prior density $\pi(\mathbf{x}_k\|\mathbf{x}_{k-1}^i, \boldsymbol{\theta})$ and then use the likelihood density to calculate the corresponding weights $\omega_k^i = \pi(\mathbf{z}_k\|\mathbf{x}_k^i, \boldsymbol{\theta})$.
Step 2
Calculate the total weight $T_\omega = \sum_{i=1}^{N} \omega_k^i$ and then normalize the particle weights, $\widehat{\omega}_k^i = \frac{\omega_k^i}{T_\omega}$.
Step 3
Resample the particles as follows: Construct the cumulative sum of weights (CSW) by computing $c_i = c_{i-1} + \widehat{\omega}_k^i$ with $c_0 = 0$. Let $i = 1$ and draw a starting point u_1 from the uniform distribution $U[0, N^{-1}]$. For $j = 1, 2, ..., N$, move along the CSW by making $u_j = u_1 + N^{-1}(j-1)$ and while $u_j > c_i$, make $i = i + 1$, assign sample $\mathbf{x}_k^j = \mathbf{x}_k^i$ and assign sample weight $\omega_k^j = N^{-1}$.

The SIR algorithm described in Tab. 1 is based on deterministic values of the model parameters. However, in some cases, the parameters may contain small uncertainties that need to be taken into account. Liu & West's algorithm can be used to estimate the posterior probability distribution $\pi(\mathbf{x}_k, \boldsymbol{\theta}|\mathbf{z}_{1:k})$, where $\boldsymbol{\theta}$ represents random parameters of the model. The Liu & West's algorithm for the particle filter is based on the hypothesis of a Gaussian mixture for the parameters vector (Liu and West, 2001; Lamien *et al.*, 2017a), given by

$$\pi(\boldsymbol{\theta}|\mathbf{z}_{1:k-1}) \approx \sum_{i=1}^{N} \omega_{k-1}^i N(\boldsymbol{\theta}|\boldsymbol{m}_{k-1}^i, \eta^2 \boldsymbol{V}_{k-1}), \tag{29}$$

where $N(.|\boldsymbol{m}, \eta^2\boldsymbol{V}_{k-1})$ is a Gaussian density with mean $\boldsymbol{m}$ and covariance matrix $\eta^2\boldsymbol{V}_{k-1}$, where η is a smoothing parameter and $\boldsymbol{V}_{k-1}$ is the covariance matrix with the parameter uncertainties. The kernel locations are specified by using the following shrinkage rule (Liu and West, 2001; Lamien *et al.*, 2017a):

$$\boldsymbol{m}_{k-1}^i = a\boldsymbol{\theta}_{k-1}^i + (1-a)\overline{\boldsymbol{\theta}}_{k-1}; \qquad a = \frac{3\delta - 1}{2\delta}, \tag{30}$$

where $a = \sqrt{1-\eta^2}$, $\overline{\boldsymbol{\theta}}_{k-1}$ is the mean of $\boldsymbol{\theta}_{k-1}$ and $0.95 < \delta < 0.99$ (Liu and West, 2001; Lamien *et al.*, 2017a).

The evolution models are obtained with the solutions of Eqs. (1) to (5). Furthermore, it is assumed here that the measurements are uncorrelated and that they contain additive Gaussian noise with zero mean and a constant covariance matrix $\boldsymbol{R}$. With such assumptions, the likelihood function used to calculate the weights is given by (Nunes *et al.*, 2019):

$$\pi(\mathbf{z}_k|\mathbf{x}_k, \boldsymbol{\theta}) = (2\pi)^{-I/2}|\boldsymbol{R}|^{-1/2} \exp\left\{ -\frac{1}{2}\left[\mathbf{z}_k^{meas} - \boldsymbol{g}_k(\mathbf{x}_k, \boldsymbol{\theta})\right]^T \boldsymbol{R}^{-1}\left[\mathbf{z}_k^{meas} - \boldsymbol{g}_k(\mathbf{x}_k, \boldsymbol{\theta})\right]\right\}, \tag{31}$$

where I is the number of measurements at each time instant t_k.

5. RESULTS AND DISCUSSIONS

With the methodologies formulated, we can now apply them to the computational solution of the problems addressed, using computational code developed in the Wolfram Mathematica® software (Wolfram, 2021).

The presentation of the results is divided into two parts. First, the direct problem is given by Eqs. (1) - (5) has been solved by applying the methodologies described in Section 3, where it will be possible to verify the results obtained with the `NDSolve` and with GITT. Next, one has the sequential estimation of the internal brain temperature containing a DBS electrode using a state estimation problem with the Particle Filter method, as described in Section 4.

Table 2. Liu & West's algorithm (Lamien *et al.*, 2017b; Liu and West, 2001)

Step 1
Find the mean $\overline{\boldsymbol{\theta}}_{k-1}$ of the parameters $\boldsymbol{\theta}$ at time t_{k-1}.
Step 2
For $i = 1, ...N$, where N is the number of particles, compute $\boldsymbol{m}_{k-1}^i$, with Eq. (30), draw new particles $\mathbf{x}_k^i$ from the prior density $\pi(\mathbf{x}_k|\mathbf{x}_{k-1}^i, \boldsymbol{m}_{k-1}^i)$ and then calculate some characterization $\boldsymbol{\mu}_k^i$ of $\mathbf{x}_k$. Use the likelihood density to calculate the corresponding weights $\omega_k^i = \omega_{k-1}^i \pi(\mathbf{z}_k|\mu_k^i, \boldsymbol{m}_{k-1}^i)$**.**
Step 3
Calculate the total weight $T_\omega = \sum_{i=1}^N \omega_k^i$ and then normalize the particle weights $\omega_k^i = \frac{\omega_k^i}{T_\omega}$.
Step 4
Resample the particles as follows: Construct the cumulative sum of weights (CSW) by computing $c_i = c_{i-1} + \omega_k^i$ with $c_0 = 0$. Let $i = 1$ and draw a starting point u_1 from the uniform distribution $U[0, N^{-1}]$. For $j = 1, 2, ..., N$, move along the CSW by making $u_j = u_1 + N^{-1}(j-1)$ and while $u_j > c_i$, make $i = i + 1$, assign sample $\mathbf{x}_k^j = \mathbf{x}_k^i$, $\boldsymbol{m}_{k-1}^j = \boldsymbol{m}_{k-1}^i$, $\boldsymbol{\mu}_k^j = \boldsymbol{\mu}_k^i$ and assign parent $i^j = i$.
Step 5
For $j = 1, 2, ..., N$ draw samples $\boldsymbol{\theta}_k^j$ from $N(\boldsymbol{\theta}_k^j|\boldsymbol{m}_{k-1}^{i^j}, \eta^2 \boldsymbol{V}_{k-1})$ by using the parent i^j.
Step 6
For $j = 1, 2, ..., N$ draw particles $\mathbf{x}_k^j$ from the prior density $\pi(\mathbf{x}_k|\mathbf{x}_{k-1}^{i^j}, \boldsymbol{\theta}_k^j$, using the parent i^j, and then use the likelihood density to calculate the correspondent weights $\omega_k^j = \pi(\mathbf{z}_k|\mathbf{x}_k^j, \theta_k^j)/\pi(\mathbf{z}_k|\boldsymbol{\mu}_k^{i^j}, \boldsymbol{m}_{k-1}^{i^j})$**.**
Step 7
Calculate the total weight $T_\omega = \sum_{j=1}^N \omega_k^j$ and then normalize the particle weights, $\omega_k^j = \frac{\omega_k^j}{T_\omega}$.

5.1 Direct problem

To obtain the solution of the direct problem, all parameters present in Eqs. (1) - (5) were considered constant and can be found in the literature as listed in Tab. 3 (Elwassif *et al.*, 2006; Jardim *et al.*, 2020). The initial temperature will be $T_a = 37°C$. The condition proposed in Eq. (5) should be defined as a step function, where the electric potential of the DBS is applied only at the position of the active electrodes. In this case, $f(z) = V_{rms}$ at the positions of the active electrodes and $f(z) = 0$ at the inactive positions, where $V_{rms} = 1.561\ V$, obtained from an electrical signal of $10\ V$, $185\ pps$ and $210\ ms$ (Elwassif *et al.*, 2006; Jardim *et al.*, 2020).

Table 3. Values of the parameters.

Parameter	Value	Parameter	Value	Parameter	Value	Parameter	Value
$T_b\ (°C)$	36.7	$R_1\ (mm)$	0.635	$\rho_b\ (kg/m^3)$	1057	$Q_m\ (W/m^3)$	9132
$\rho\ (kg/m^3)$	1040	$R_2\ (mm)$	20.0	$c_b\ (J/kgK)$	3600	$\sigma\ (S/m)$	0.35
$c_p\ (J/kgK)$	3650	$H\ (mm)$	50.0	$\omega_b\ (ml/scm^3)$	0.008	$k\ (W/mK)$	0.527

First, the solution for the electric potential, Eqs. (4) and (5), and for the temperature, Eqs. (1) and (2), were obtained with the routine `NDSolve`, choosing as method of solution the Finite Element Method (FEM) with a mesh composed of 5832 triangular elements, generated with the option `MaxCellMeasure` included in the routine `NDSolve`. Then the solution was found using separation of variables, for the electric potential with 300 eigenvalues, and GITT, for the temperature with 400 eigenvalues where `NDSolve` was used to solve the system of coupled PDEs. The comparison between the solutions, with electrodes 1 and 4 actives of the Model 3387, can be seen in Fig 2 where it is observed that the solutions show good agreement. The codes were run on an Intel(R) Core(TM) processor i7-8550U@1.80GHz with 8 GB of RAM. The `NDSolve` solution was obtained with less than one minute and the solution by GITT took about 14 hours, so the `NDSolve` solution was chosen and used in the inverse problems shown in the next section.

5.2 Inverse problem

After solving the direct problem, 61 simulated experimental temperature measurements were obtained every one second at the sensor position in Fig. 1(a), using a normal distribution with zero mean and constant standard deviation, ε. Two different noise levels were analyzed, being the standard deviation of $\varepsilon = 0.05\ °C$ and subsequently $\varepsilon = 0.2\ °C$. The choice of uncertainties in the evolution and observation models were, for simplicity, arbitrarily assumed to be additive, Gaussian, uncorrelated and with zero mean, as usually found in the literature related to bioheat transfer (Lamien *et al.*,

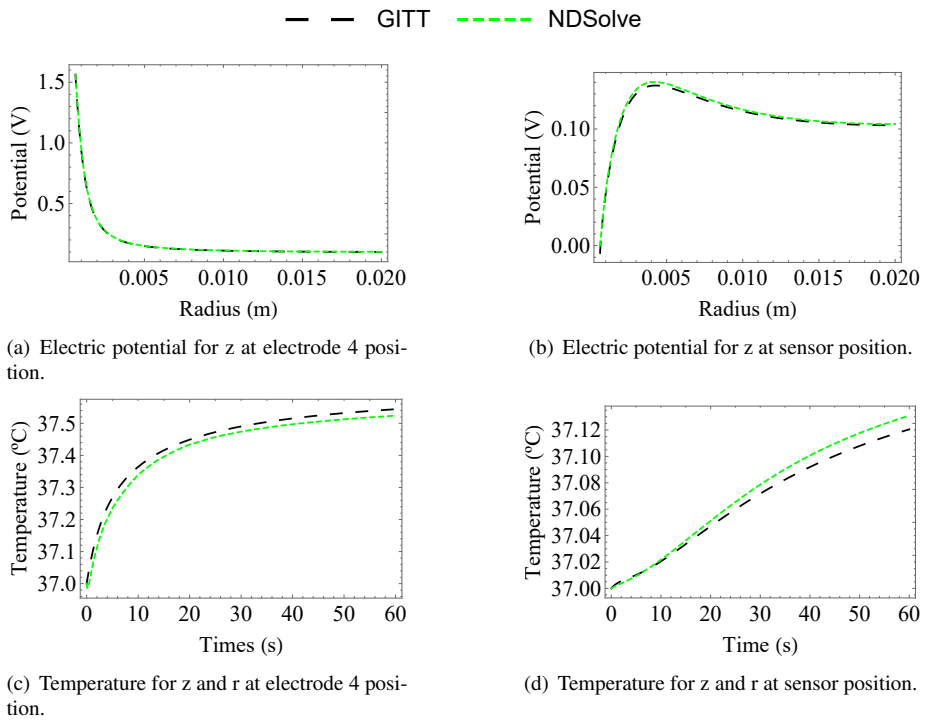

(a) Electric potential for z at electrode 4 position.

(b) Electric potential for z at sensor position.

(c) Temperature for z and r at electrode 4 position.

(d) Temperature for z and r at sensor position.

Figure 2. Comparison between `NDSolve` and GITT solutions.

2017b; Nunes *et al.*, 2020, 2019; Pacheco *et al.*, 2018; Lamien *et al.*, 2017a). The standard deviation for the evolution model, as well as for the observation model, was $0.05\ ^{\circ}C$. Furthermore, the heat source term resulting from the heating was considered with additive Gaussian noise and its evolution model is given by (Lamien *et al.*, 2017b):

$$Q^i_{ext,k}(r,z) = Q^i_{ext,k-1}(r,z) + \epsilon^i_k(r,z), \tag{32}$$

$\epsilon^i_k(r,z)$ has mean zero and standard deviation 1% of $Q^i_{ext,k-1}(r,z)$. For SIR algoritm, the vector $\boldsymbol{\theta}$ is assumed to be known, but the related uncertainties are accounted for in the noise vectors v_k and n_k. In Liu & West's algorithm, on the other hand, the parameters are assumed to have a standard deviation of $1\ \%$ of the values listed in Tab. 3. To verify the effect of the number of particles used in the algorithms the root mean square error between the estimated and exact temperatures was used for this propose, which is given by (Lamien *et al.*, 2017b; Nunes *et al.*, 2019):

$$RMS = \frac{\sqrt{\sum_{p=1}^{P}\left(T_{est,p} - T_{exa,p}\right)^2}}{P}, \tag{33}$$

where $T_{est,p}$ and $T_{exa,p}$ denote, respectively, the estimated and exact temperatures obtained with the sensor, and $P = 61$ the total number of time steps where the temperatures were compared.

In Tab. 4 are the results for SIR algorithm with $N = 100$, $N = 250$ and $N = 500$ particles, electrodes 1 and 4 of Model 3387 active and two different noise levels, $\varepsilon = 0.05\ ^{\circ}C$ and $\varepsilon = 0.2\ ^{\circ}C$. The RMS errors are reported in terms of their mean and standard deviation values, obtained with 10 runs of each algorithm, to avoid any bias resulting from the simulated measurements. Computational times refer to a single run of the executed codes. Observing Tab. 4 is possible to verify that when increasing the number of particles, the CPU time increases, and the RMS error does not present many variations. It also is seen that by increasing the noise in the simulated experimental measurements of temperatures, the RMS error also increases. By choosing $N = 250$ the estimated temperature profiles over time were obtained for the two models with different pairs of active electrodes, as can be seen in Figs. 3 and 4, where it is observed that the temperature field was accurately estimated for both electrodes with different active positions, despite the uncertainties in the evolution and observation models. Moreover, even when increasing the noise level, good results were found.

For the Liu & West algorithm, first results were obtained for Model 3387 with $N = 100$ and $N = 250$ particles and $\varepsilon = 0.05^{\circ}C$. The results with $N = 100$ were with RMS error of $3.09 \times 10^{-3}\ ^{\circ}C$ and CPU time around 7 hours. The results for $N = 250$ were with RMS error of $2.23 \times 10^{-3}\ ^{\circ}C$ and CPU time of 30 hours. For this reason, 100 particles were used to obtain the results shown in Fig. 5, obtained for Models 3387 and 3399 with electrodes 2 and 3 active considering different noise levels in the experimental data. It can be seen that this algorithm can accurately estimate the temperature even when adding uncertainties to the parameters, which is an important point because it allows future estimation of some brain parameters to take into account the differences in thermal properties that occur between patients.

Table 4. RMS errors and CPU time for SIR algorithm.

ε ($^\circ C$)	Number of particles	RMS error mean ($^\circ C$)	RMS error standard desviation ($^\circ C$)	CPU time (min)
0.05	100	2.07×10^{-3}	7.66×10^{-5}	13
	250	2.03×10^{-3}	2.72×10^{-5}	29
	500	2.00×10^{-3}	3.05×10^{-5}	65
0.20	100	2.50×10^{-2}	3.08×10^{-3}	13
	250	2.42×10^{-2}	2.89×10^{-3}	29
	500	2.31×10^{-2}	2.81×10^{-3}	65

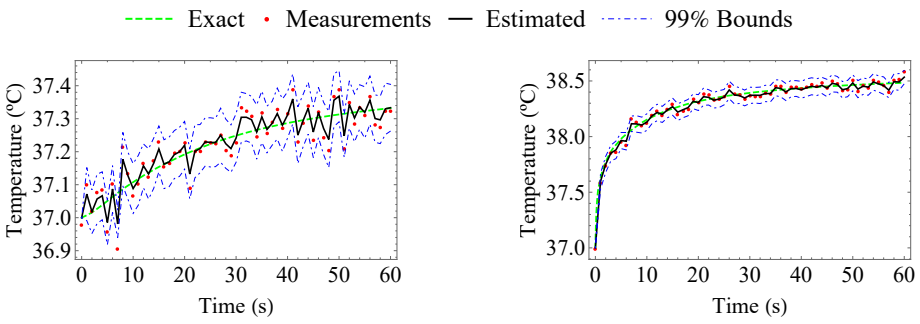

(a) Model 3389 and electrodes 1 and 4 actives.

(b) Model 3389 and electrodes 2 and 3 actives.

(c) Model 3387 and electrodes 1 and 4 actives.

(d) Model 3387 and electrodes 2 and 3 actives.

Figure 3. The solution of the state estimation problem at sensor position for $\varepsilon = 0.05^\circ C$ with the SIR algorithm.

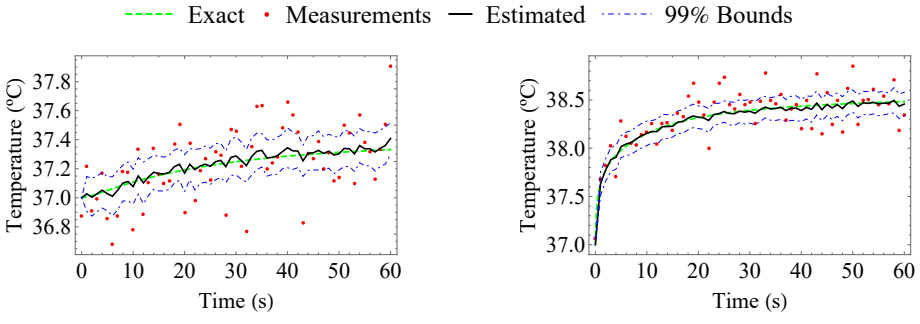

(a) Model 3389 and electrodes 1 and 4 actives.

(b) Model 3389 and electrodes 2 and 3 actives.

(c) Model 3387 and electrodes 1 and 4 actives.

(d) Model 3387 and electrodes 2 and 3 actives.

Figure 4. The solution of the state estimation problem at sensor position for $\varepsilon = 0.2^\circ C$ with the SIR algorithm.

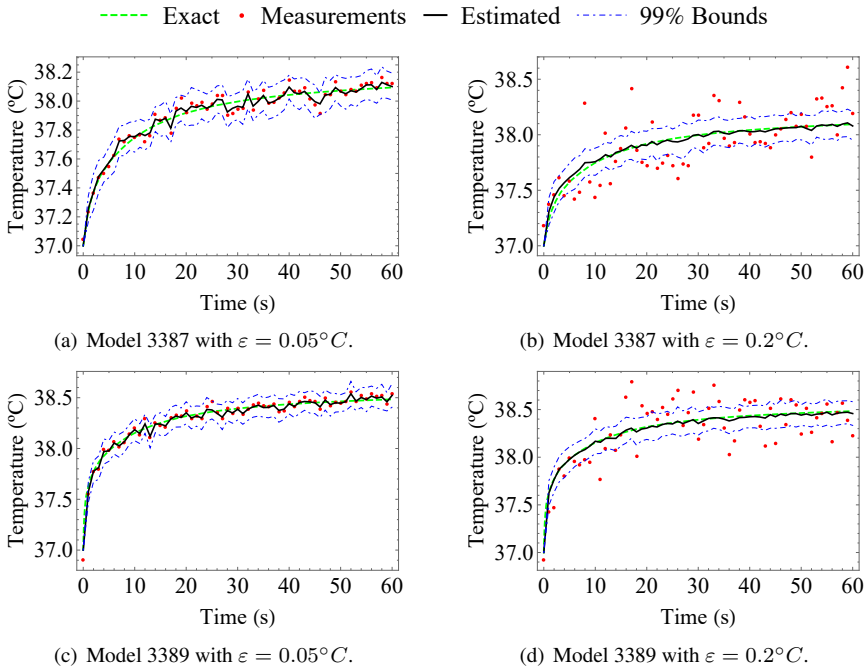

(a) Model 3387 with $\varepsilon = 0.05°C$.

(b) Model 3387 with $\varepsilon = 0.2°C$.

(c) Model 3389 with $\varepsilon = 0.05°C$.

(d) Model 3389 with $\varepsilon = 0.2°C$.

Figure 5. The solution of the state estimation problem at sensor position for Liu & West's algorithm.

6. CONCLUSION

This paper dealt with the solution of state estimation problems related to DBS electrical activity in the brain. First, the associated direct problem was solved with a finite element approach implemented using the function `NDSolve` and verified with GITT to acquire more confidence in the presented result. The inverse problem was developed to improve the accuracy of the estimated temperature field taking into account as many uncertainties as possible. Simulated temperature measurements from a single sensor within the domain were used for this purpose. The SIR and Liu & West algorithms, which takes into account the uncertainties in the evolution and observation models and the measurements, were used. The results show that the estimated temperatures were in excellent agreement with the exact temperatures for the two DBS electrodes examined, considering different combinations of active electrodes and different noise levels in the simulated experimental measurements. Therefore, the solutions presented showed a promising approach to reduce the risk of injury related to the deep brain stimulation technique.

7. ACKNOWLEDGEMENTS

This study was financed in part by the Coordenação de Aperfeiçoamento de Pessoal de Nível Superior - Brasil (CAPES) - Finance Code 001, the Conselho Nacional de Desenvolvimento Científico e Tecnológico (CNPq) and the Fundação Carlos Chagas Filho de Amparo à Pesquisa do Estado do Rio de Janeiro (FAPERJ).

8. REFERENCES

Aum, D.J. and Tierney, T.S., 2018. "Deep brain stimulation foundations and future trends". *Frontiers in Bioscience*, Vol. 23, No. 7, p. 162–182.

Chang, I., 2003. "Finite element analysis of hepatic radiofrequency ablation probes using temperature-dependent electrical conductivity". *Biomedical engineering online*, Vol. 2, No. 1, pp. 1–18.

Cotta, R.M., Knupp, D.C., Naveira-Cotta, C.P., Sphaier, L.A. and Quaresma, J.N.N., 2013. "Unified integral transforms algorithm for solving multidimensional nonlinear convection-diffusion problems". *Numerical Heat Transfer, Part A: Applications*, Vol. 63, No. 11, pp. 840–866.

Cotta, R.M., Knupp, D.C. and Quaresma, J.N.N., 2018. *Analytical methods in heat transfer*. Kulacki F. (eds) Handbook of Thermal Science and Engineering. Springer International Publishing.

Cubo, R. and Medvedev, A., 2018. "Online tissue conductivity estimation in deep brain stimulation". *IEEE Transactions on Control Systems Technology*, Vol. 28, No. 1, pp. 149–162.

Elwassif, M.M., Datta, A., Rahman, A. and Bikson, M., 2012. "Temperature control at dbs electrodes using a heat sink: experimentally validated fem model of dbs lead architecture". *Journal of Neural Engineering*, Vol. 9, No. 4, p. 046009.

Elwassif, M.M., Kong, Q., Varquez, M. and Bikson, M., 2006. "Bio-heat transfer model of deep brain stimulation-induced

temperature changes". *Journal of Neural Engineering*, Vol. 3, No. 4, pp. 306–315.

Fiocchi, S., Bonato, G.M., Chiaramello, E., Gallucci, S., Tognola, G., Ravazzani, P. and Parazzini, M., 2020. "Numerical modelling of temperature increase induced by transcutaneous spinal direct current stimulation (tsdc)". In *IEEE 20th Mediterranean Electrotechnical Conference - MELECON 2020*.

Jardim, L.C.S., Abreu, L.A.S., Knupp, D.C. and Neto, A.J.S., 2020. "Brain thermal and electrical properties estimation using experimental data from deep brain stimulation lead". *Revista Mundi Engenharia, Tecnologia e Gestão*, Vol. 5, No. 6, pp. 291–01,291–15.

Khadka, N., Harmsen, I.E., Lozano, A.M. and Bikson, M., 2020. "Bio-heat model of kilohertz-frequency deep brain stimulation increases brain tissue temperature". *Neuromodulation: Technology at the Neural Interface*, Vol. 23, No. 4, pp. 489–495.

Krauss, J.K., Yianni, J., Loher, T.J. and Aziz, T.Z., 2004. "Deep brain stimulation for dystonia". *Journal of Clinical Neurophysiology*, Vol. 21, No. 1, pp. 18–30.

Lam, J., Lee, J., Liu, C.Y., Lozano, A.M. and Lee, D.J., 2021. "Deep brain stimulation for alzheimer's disease: Tackling circuit dysfunction". *Neuromodulation: Technology at the Neural Interface*, Vol. 24, No. 2, pp. 171–186.

Lamien, B., Orlande, H.R.B. and Eliçabe, G.E., 2017a. "Particle filter and approximation error model for state estimation in hyperthermia". *Journal of Heat Transfer*, Vol. 139, No. 1, pp. 012001–3.

Lamien, B., Varon, L.A.B. and Orlande, H.R.B., 2017b. "State estimation in bioheat transfer: a comparison of particle filter algorithms". *International Jornal of Numerical Methods for Heat & Fluid Flow*, Vol. 27, No. 3, pp. 615–638.

Liu, J. and West, M., 2001. *Combined Parameter and State Estimation in Simulation-Based Filtering*. Sequential Monte Carlo Methods in Practice, A. Doucet, N. de Freitas, and N. Gordon, eds. Springer, New York.

Medtronic and INC, 2002. *DBS Lead Kit for Deep Brain Stimulation, Model 3387/3389*. Minneapolis, MN, US: [s.n.].

Mikhailov, M.D. and Ozisik, M.N., 1984. *Unified analysis and solutions of heat and mass diffusion*. John Wiley & Sons, New York.

Nunes, F.S.A., Magalhães, F.Y., Da Silva, N.P. and Orlande, H.R.B., 2020. "State estimation using the optimal sequential bayenian filter in bioheat transfer applications". In *18th Brazilian Congress of Thermal Sciences and Engineering - ENCIT 2020*. Online.

Nunes, F.S.A., Orlande, H.R.B. and Nowak, A.J., 2019. "Estimation of the ischemic brain temperature with the particle filter method". *Journal of Mechanisms and Robotics*, Vol. 26, No. 1, pp. 5–19.

Orlande, H.R.B., Dulikravich, G.S. and Colaço, M.J., 2008. "Application of bayesian filters to heat conduction problems". In *International Conference on Engineering Optimization - EngOpt 2008*. Rio de Janeiro, Brazil.

Orlande, H.R.B., Dulikravich, G.S., Colaço, M.J., Vianna, G.S., Da Silva, F.L.V., Fonseca, H.M. and Fudym, O., 2011. "Tutorial 10 kalman and particle filters". *Advanced Spring School: Thermal measurements and inverse techniques*, Vol. 5, pp. 1–39.

Pacheco, C., Orlande, H.R.B., Colaço, M.J. and Dulikravich, G.S., 2018. "State estimation problems in prf-shift magnetic resonance thermometry". *International Journal of Numerical Methods for Heat & Fluid Flow*, Vol. 28, No. 2, pp. 315–335.

Pacheco, C., Orlande, H.R.B., Colaço, M.J., Dulikravich, G.S., Varon, L.A. and Lamien, B., 2020. "Real-time temperature estimation with enhanced spatial resolution during mr-guided hyperthermia therapy". *Numerical Heat Transfer, Part A: Applications*, Vol. 77, No. 8, pp. 782–806.

Pennes, H.H., 1948. "Analysis of tissue arterial blood temperature in the resting forearm". *Journal of Applied Physiology*, Vol. 1, No. 2, p. 93–122.

Salanova, V., 2018. "Deep brain stimulation for epilepsy". *Epilepsy & Behavior*, Vol. 88, pp. 21–24.

Starr, P.A., Vitek, J.L. and Bakay, R.A., 1998. "Ablative surgery and deep brain stimulation for parkinson's disease". *Neurosurgery*, Vol. 43, No. 5, pp. 989–1013.

Wolfram, 2021. "Wolfram language & system: Documentation center". https://reference.wolfram.com/language/. Accessed 11 June 2021.

Xiao, Y., Lau, J.C., Hemachandra, D., Gilmore, G., Khan, A.R. and Peters, T.M., 2020. "Image guidance in deep brain stimulation surgery to treat parkinson's disease: a review". *arXiv preprint arXiv:2003.04822*.

9. RESPONSIBILITY NOTICE

The authors are solely responsible for the printed material included in this paper.